Improved Branching Ratio Measurement for the Decay $K_L^0 \to \mu^+\mu^-$

D. Ambrose,[1] C. Arroyo,[2] M. Bachman,[3] D. Connor,[3] M. Eckhause,[4] S. Graessle,[1] A. D. Hancock,[4] K. Hartman,[2] M. Hebert,[2] C. H. Hoff,[4] G. W. Hoffmann,[1] G. M. Irwin,[2] J. R. Kane,[4] N. Kanematsu,[3] Y. Kuang,[4] K. Lang,[1] R. Lee,[3] R. D. Martin,[4] J. McDonough,[1] A. Milder,[1] W. R. Molzon,[3] M. Pommot-Maia,[2] P. J. Riley,[1] J. L. Ritchie,[1] P. D. Rubin,[5] V. I. Vassilakopoulos,[1] R. E. Welsh,[4] and S. G. Wojcicki[2]

(BNL E871 Collaboration)

[1]*University of Texas, Austin, Texas 78712*
[2]*Stanford University, Stanford, California 94305*
[3]*University of California, Irvine, California 92697*
[4]*College of William and Mary, Williamsburg, Virginia 23187*
[5]*University of Richmond, Richmond, Virginia 23173*

(Received 24 August 1999)

We report results from Experiment 871, performed at the BNL AGS, of a measurement of the branching ratio $K_L^0 \to \mu^+\mu^-$ with respect to the *CP*-violating mode $K_L^0 \to \pi^+\pi^-$. This experiment detected over 6200 candidate $\mu^+\mu^-$ events, a factor of 6 more than that seen in all previous measurements combined. The resulting branching ratio $\Gamma(K_L^0 \to \mu^+\mu^-)/\Gamma(K_L^0 \to \pi^+\pi^-) = (3.474 \pm 0.057) \times 10^{-6}$ leads to a branching fraction $B(K_L^0 \to \mu^+\mu^-) = (7.18 \pm 0.17) \times 10^{-9}$, which is consistent with the current world average, and reduces the uncertainty in this decay mode by a factor of 3.

PACS numbers: 13.20.Eb, 12.15.Hh, 12.15.Mm

We report an improved branching ratio measurement for the rare decay $K_L^0 \to \mu^+\mu^-$. It was the low rate of this decay which led in part to the proposal of the Glashow-Illiopoulos-Maiani mechanism [1] and a fourth quark (charm) whose presence cancels flavor-changing neutral currents at tree level, and strongly suppresses second-order loop diagrams with the up quark. The decay rate is saturated by an absorptive process with a real, two-photon intermediate state, which is determined from a QED calculation [2] for $\Gamma(K_L^0 \to \gamma\gamma \to \mu^+\mu^-)/\Gamma(K_L^0 \to \gamma\gamma)$ and the measured $K_L^0 \to \gamma\gamma$ branching fraction [3]. This contribution, referred to as the "unitarity bound," equals $(7.07 \pm 0.18) \times 10^{-9}$, and establishes the minimum rate expected for $K_L^0 \to \mu^+\mu^-$.

The residual dispersive amplitude for the $\mu^+\mu^-$ decay rate contains contributions from second-order electroweak (short-distance) diagrams and a long-distance electromagnetic part. The former are dominated by the heavy top quark, so that $B(K_L^0 \to \mu^+\mu^-)_{\mathrm{SD}}$ is approximately proportional to $|\mathrm{Re}(V_{ts}^* V_{td})|^2$ [4], or to $(\rho_0 - \bar{\rho})^2$ [5] in the Wolfenstein parametrization of the Cabibbo-Kobayashi-Maskawa (CKM) quark mixing matrix [6]. Our ability to extract information on ρ from the $\mu^+\mu^-$ branching fraction is currently limited by theoretical uncertainties [7–9] in the calculation of the long-distance contributions.

The major backgrounds for $K_L^0 \to \mu^+\mu^-$ arise from the semileptonic decays $K_L^0 \to \pi^\pm\mu^\mp\nu$ ($K_{\mu 3}$) and $K_L^0 \to \pi^\pm e^\mp\nu$ (K_{e3}), with subsequent pion decay and electron (from K_{e3}) misidentification. These backgrounds are suppressed by cuts on the net transverse momentum (p_T) of the charged decay products, which is zero for two-body decays and nonzero for semileptonics. At low neutrino momentum, the reconstructed $\mu^+\mu^-$ mass of $K_{\mu 3}$ events approaches 489 MeV/c^2, 8 MeV/c^2 below the K_L^0 mass, requiring good momentum and mass resolution to suppress this background. K_{e3} events misidentified as $\mu^+\mu^-$ may give a two-body mass above the K_L^0 mass, so that good muon identification and electron rejection are also needed.

Brookhaven National Laboratory (BNL) Experiment 871 recorded data in 1995 and 1996 at the B5 beam line of the Alternating Gradient Synchrotron (AGS), and significantly improved upon BNL E791 [10], which observed about 700 $\mu^+\mu^-$ events. The experimental apparatus has been described previously [11,12]. Briefly, a high flux neutral beam was produced by 24 GeV protons incident on a Pt target. Defined by a series of sweeping magnets and collimators, the beam then entered a vacuum decay tank with a roughly 11 m fiducial length. Decay particles exiting the tank proceeded through a double-magnet spectrometer with six pairs of drift chambers [13]. The neutral beam terminated in a beam stop [14] located within the first magnet. The magnets had opposite polarity giving a net p_T kick inwards of $\sim$200 MeV/c, causing particles from two-body decays to emerge from the spectrometer with roughly parallel trajectories.

Signals from two banks of narrow-slat trigger scintillator (TSC) hodoscopes provided a minimum bias Level 0 trigger, selecting parallel, two-track events. Two muon hodoscope (MHO) modules placed downstream of a 46 cm iron filter were aligned with the TSC counters to form Level 1 $\mu^+\mu^-$ triggers. Level 0 triggers, prescaled by a factor of 2000, allowed simultaneous measurement of $\pi^+\pi^-$ events for normalization. A software trigger (Level 3) used information from the drift chambers and TSC counters to select events with a vertex within the decay volume, and to apply loose cuts on $\mu^+\mu^-$ mass and p_T. Offline analysis used electron identification from a lead glass (PBG) calorimeter and muon identification from

a muon range finder (MRG). The MRG, consisting of proportional counters interspersed between slabs of iron, marble, and aluminum, combined with four additional MHO modules to achieve a 5% range measurement.

The analysis began with a pattern recognition algorithm using drift chamber hits to reconstruct tracks on each side of the spectrometer. This information was then processed by two independent fitting algorithms that used a 3-dimensional magnetic field map to determine the final kinematic quantities: invariant mass, p_T, vertex position, and track 3-momenta. The first fitter (FT) minimized the χ^2 for a global fit of each track, incorporating multiple-scattering and resolution effects. FT gave mass resolutions for $\mu^+\mu^-$ and $\pi^+\pi^-$ events of 1.26 and 1.11 MeV/c^2, respectively. A second algorithm (QT) used an iterative approach to determine track kinematics independently for the upstream and downstream halves of the spectrometer, leading to $\mu^+\mu^-$ and $\pi^+\pi^-$ mass resolutions of 1.43 and 1.25 MeV/c^2. Tracks exiting the spectrometer were then projected to the downstream detectors to check for associated hits.

Only events successfully reconstructed by both algorithms (approximately 87% of the $\mu^+\mu^-$ data sample) were retained, after which subsequent FT and QT analyses proceeded in parallel. Loose cuts were placed on the fitter χ^2 values to achieve good efficiency ($\sim$99%) and minimize systematic errors. The decay vertex was required to fall inside the neutral beam profile defined by the collimators and within 9.55–20.6 m along the beam line (z direction). Track momentum was constrained between 1.05–6.5 GeV/c. Finally, a signal region was defined with an invariant mass range of 493.5–502.0 MeV/c^2 for FT and 493.0–502.5 MeV/c^2 for QT, and with p_T^2 below 100 (MeV/c)^2, corresponding to roughly 3σ in mass and p_T resolution.

K_{e3} contamination was greatly reduced by using PBG energy measurement to reject tracks consistent with being electrons ($E/p \approx 1$). Muons were identified by demanding consistency of MHO phototube times, and a range from the MHO/MRG track hits at least 80% of the predicted range to suppress muons from $K_{\mu 3}$ and K_{e3} pion decay. The projected tracks were also required to coincide spatially with in-time TSC trigger hits. Backgrounds from multiple decays were reduced by a factor of 2 through demanding only one set of track-associated parallel hits in each side of the TSC.

Figure 1(a) shows (for the FT fitter) the reconstructed mass for the $\mu^+\mu^-$ data sample after applying all kinematic and particle identification cuts. A $\mu^+\mu^-$ signal peak at the K_L^0 mass is well separated from the $K_{\mu 3}$ background, which declines rapidly to the kinematic limit near 489 MeV/c^2. Figure 1(b) shows the FT fitter p_T^2 for the $\mu^+\mu^-$ sample after cuts. To subtract background, a linear fit was performed to the sideband region 150–700 (MeV/c)^2 of the p_T^2 distribution, and extrapolated under the signal peak, yielding over 6200 candidate $\mu^+\mu^-$ events ($N_{\mu\mu}$ in Table I) with a background level of

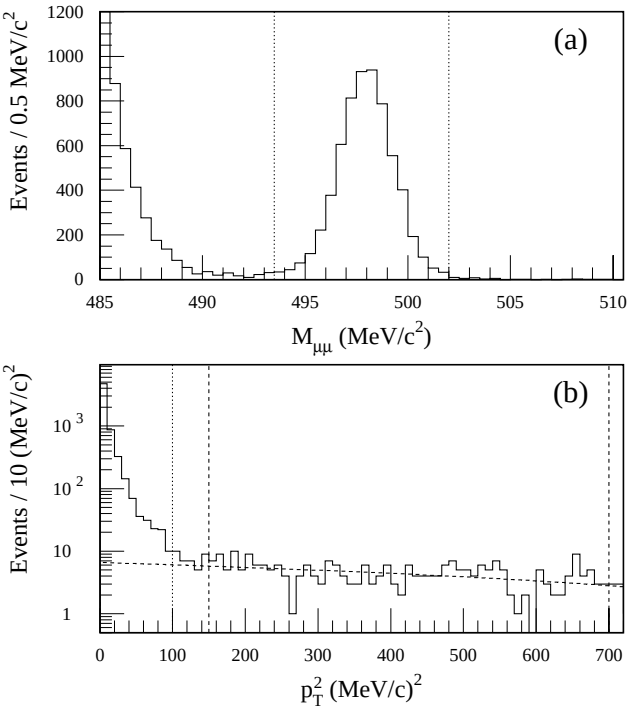

FIG. 1. Reconstructed invariant $\mu^+\mu^-$ mass (a) and p_T^2 (b), the latter showing the linear background subtraction. Vertical lines denote the signal (dotted) and fitting (dashed) regions.

1.0% for FT and 1.3% for QT. A roughly 20% variation on the background count was observed by adjusting the sideband boundaries, and incorporated into the total signal error, giving an uncertainty on $N_{\mu\mu}$ of 1.3%.

With the exception of muon identification, identical cuts were applied to the $\pi^+\pi^-$ normalization sample to minimize potential systematic errors. $K_{\mu 3}$ decays have a kinematic limit on reconstructed $\pi^+\pi^-$ mass $\sim$8 MeV/c^2 above the K_L^0 mass, and thus contribute to the $K_L^0 \to \pi^+\pi^-$ sample. This background was subtracted by using Monte Carlo $K_{\mu 3}$ distributions normalized to the mass and p_T^2 sidebands, as shown in Fig. 2 for the FT fitter. The sidebands chosen were 475–480 and 505–520 MeV/c^2 for the mass, and 150–600 (MeV/c)^2 in p_T^2. The number of $\pi^+\pi^-$ events $N_{\pi\pi}$ was taken as the central value of the

TABLE I. Candidate event numbers, Monte Carlo and efficiency-weighted acceptances, and resultant branching ratios ($\times 10^{-6}$) for the FT and QT fitters. Brackets indicate fractional uncertainties (in percent).

	FT		QT	
$N_{\mu\mu}$	6216 ± 81	[1.30]	6205 ± 82	[1.32]
$N_{\pi\pi}$	798754 ± 2261	[0.28]	791073 ± 2249	[0.28]
$A_{\mu\mu}$	0.01779 ± 0.00002	[0.11]	0.01780 ± 0.00002	[0.11]
$A_{\pi\pi}$	0.01586 ± 0.00002	[0.13]	0.01578 ± 0.00002	[0.13]
$A'_{\mu\mu}$	0.01463 ± 0.00007	[0.48]	0.01464 ± 0.00007	[0.47]
$A'_{\pi\pi}$	0.01405 ± 0.00008	[0.57]	0.01398 ± 0.00008	[0.57]
$A^{\pi\pi}_{\mu\mu}$	0.9606 ± 0.0091	[0.95]	0.9549 ± 0.0084	[0.88]
$B^{\mu\mu}_{\pi\pi}$	3.471 ± 0.057	[1.64]	3.477 ± 0.056	[1.61]

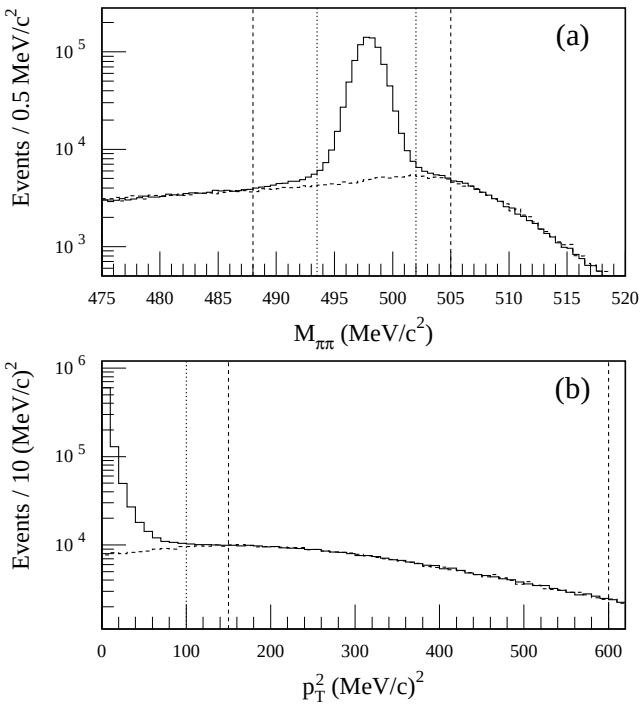

FIG. 2. Reconstructed invariant $\pi^+\pi^-$ mass (a) and p_T^2 (b) for the data (solid histogram) and Monte Carlo $K_{\mu 3}$ background (dashed histogram). Vertical lines denote the signal (dotted) and normalization (dashed) regions.

mass and p_T^2 subtraction methods. The 0.5% difference in signal found between methods was interpreted as a systematic error in the Monte Carlo, leading to a total uncertainty on $N_{\pi\pi}$ of approximately 0.3% (see Table I). Contamination from $K_S^0 \to \pi^+\pi^-$ decays and K_L^0-K_S^0 interference was calculated to be below 10^{-4} after application of the track momenta and vertex z-position cuts.

The ratio for the $K_L^0 \to \mu^+\mu^-$ rate with respect to $K_L^0 \to \pi^+\pi^-$ was determined from the numbers of candidate events, $N_{\mu\mu}$ and $N_{\pi\pi}$, according to

$$B_{\pi\pi}^{\mu\mu} = \frac{1}{P}\,\frac{N_{\mu\mu}}{N_{\pi\pi}}\,\frac{A_{\pi\pi}}{A_{\mu\mu}}\,\frac{1}{\varepsilon_{\mu\mu}^{\mathrm{L1}}}\,\frac{1}{\varepsilon_{\mu\mu}^{\mathrm{L3}}}\,\frac{\varepsilon_{\pi\pi}^{\mathrm{TSC}}}{\varepsilon_{\mu\mu}^{\mathrm{TSC}}}\,\frac{\varepsilon_{\pi\pi}^{\mathrm{veto}}}{\varepsilon_{\mu\mu}^{\mathrm{veto}}}\,\frac{\varepsilon_{\pi\pi}^{\mathrm{ABS}}}{\varepsilon_{\mu\mu}^{\mathrm{PID}}},$$

where P denotes the prescale factor applied to the $\pi^+\pi^-$ normalization sample, and $A_{\mu\mu}$ and $A_{\pi\pi}$ are the Monte Carlo simulated acceptances, which correct for the mode-dependent efficiencies of the detector apparatus and kinematic cuts. The quantities ε are the mode-dependent trigger and particle identification efficiencies: $\varepsilon_{\mu\mu}^{\mathrm{L1}}$ and $\varepsilon_{\mu\mu}^{\mathrm{L3}}$ are the $\mu^+\mu^-$ hardware and software trigger efficiencies, $\varepsilon_{\mu\mu}^{\mathrm{TSC}}$ and $\varepsilon_{\pi\pi}^{\mathrm{TSC}}$ are the efficiencies of the TSC space match, track-time, and track-number cuts, $\varepsilon_{\mu\mu}^{\mathrm{veto}}$ and $\varepsilon_{\pi\pi}^{\mathrm{veto}}$ are the PBG electron veto efficiencies, $\varepsilon_{\mu\mu}^{\mathrm{PID}}$ equals the MHO/MRG $\mu^+\mu^-$ particle identification efficiency, and the quantity $\varepsilon_{\pi\pi}^{\mathrm{ABS}}$ corrects for the loss of $\pi^+\pi^-$ events from hadronic absorption in the detectors. To prevent biasing our analysis through knowledge of previous measurements or theoretical expectations, an additional, random prescale factor of 90%–95% was applied to the normalization sample in software, and revealed only after all analysis cuts, Monte Carlo acceptances, and efficiency terms were frozen [15], giving a total prescale P of 2154.

To determine the $\mu^+\mu^-$ and $\pi^+\pi^-$ acceptances (see Table I), 10^6 Monte Carlo events for each decay mode were analyzed to calculate losses due to spectrometer geometrical acceptance, wire inefficiencies, pattern recognition, and fitter cuts. A software Level 0 trigger was then applied by demanding hits in the TSC within the $\pm$2-slat parallelism window. The Monte Carlo also simulated the TSC counter efficiencies, which were measured as a function of position along the slat from single-track trigger data. In addition to these cuts, the Monte Carlo simulated the radiative decays for $\mu^+\mu^-$ and $\pi^+\pi^-$ events [16,17], which caused approximately 1.0% of $\mu^+\mu^-$ and 0.9% of $\pi^+\pi^-$ events to escape the signal region.

The mode-dependent efficiencies ε were measured from data and used to correct the acceptances for trigger and particle-ID inefficiencies not incorporated in the Monte Carlo. Except for $\varepsilon_{\mu\mu}^{\mathrm{L1}}$, these efficiencies are functions of kinematic variables, e.g., track momentum, and represent weights applied to the Monte Carlo samples event-by-event. Table II shows the integrated values for each ε, along with their total uncertainties combining the propagated statistical errors from each bin with estimated systematic uncertainties. The combined total efficiencies $\varepsilon^{\mathrm{tot}}$ differ from the products of efficiencies due to correlations, which increase the $\pi^+\pi^-$ efficiency by 0.45% and decrease the $\mu^+\mu^-$ result by 0.17%. The uncertainties for individual efficiencies are expected to be uncorrelated, and hence are added in quadrature with the Monte Carlo acceptance uncertainty. The resulting efficiency-weighted acceptances $A'_{\mu\mu}$ and $A'_{\pi\pi}$ are shown in Table I.

Level 1 $\mu^+\mu^-$ triggers demanded parallel MHO signals in coincidence with Level 0. The efficiency $\varepsilon_{\mu\mu}^{\mathrm{L1}}$ for this additional trigger requirement was measured from $K_{\mu 3}$ events, where the pion decayed to produce two muons at the MHO, and was found to be independent of track kinematics. The efficiency of the $\mu^+\mu^-$ Level 3 software trigger was studied using $\pi^+\pi^-$ events, and showed a dependence on track bending angle in the analyzing magnets due to the momentum-dependent search windows of the Level 3 reconstruction algorithm. To account for this

TABLE II. Trigger and particle identification efficiencies for $\mu^+\mu^-$ and $\pi^+\pi^-$ decays (integrated separately), and the combined total efficiencies of the weight functions. Brackets indicate fractional uncertainties (in percent).

$\varepsilon_{\mu\mu}^{\mathrm{L1}}$	0.9714 ± 0.0021	[0.22]	⋯	⋯	⋯
$\varepsilon_{\mu\mu}^{\mathrm{L3}}$	0.9302 ± 0.0021	[0.23]	⋯	⋯	⋯
$\varepsilon_{\mu\mu}^{\mathrm{TSC}}$	0.9788 ± 0.0021	[0.21]	$\varepsilon_{\pi\pi}^{\mathrm{TSC}}$	0.9501 ± 0.0018	[0.19]
$\varepsilon_{\mu\mu}^{\mathrm{veto}}$	0.9957 ± 0.0012	[0.12]	$\varepsilon_{\pi\pi}^{\mathrm{veto}}$	0.9784 ± 0.0012	[0.12]
$\varepsilon_{\mu\mu}^{\mathrm{PID}}$	0.9357 ± 0.0019	[0.20]	$\varepsilon_{\pi\pi}^{\mathrm{ABS}}$	0.9480 ± 0.0047	[0.50]
$\varepsilon_{\mu\mu}^{\mathrm{tot}}$	0.8223 ± 0.0037	[0.45]	$\varepsilon_{\pi\pi}^{\mathrm{tot}}$	0.8856 ± 0.0048	[0.54]

small mode dependence, the Level 3 efficiency was binned by bending angle, giving a value for $\varepsilon_{\mu\mu}^{\mathrm{L3}}$ 0.7% lower than the efficiency measured directly for the $\pi^+\pi^-$ sample.

The efficiency functions $\varepsilon^{\mathrm{TSC}}$ and $\varepsilon^{\mathrm{veto}}$ were measured as a function of momentum from muons and pions in minimum bias events. The mode dependence for the TSC cuts resulted from the application of the Level 3 software trigger to the $\mu^+\mu^-$ sample, which checked for parallel hits in the trigger scintillators. The electron veto mode dependence originated from pions inducing hadronic interactions in the PBG, which could mimic electromagnetic showers. The muon identification efficiency $\varepsilon_{\mu\mu}^{\mathrm{PID}}$ was also measured with minimum bias muons, and binned by both track momentum and horizontal x position at the MRG.

To account for the loss of $\pi^+\pi^-$ events from hadronic interactions upstream of the final TSC module, a GEANT calculation was performed simulating the detector materials. The absorption probability was parametrized by momentum to form the $\varepsilon_{\pi\pi}^{\mathrm{ABS}}$ weight function, with an assumed 8% systematic uncertainty in detector mass and cross section data. The resulting value of absorption loss was checked by comparing the calculated loss due to detector materials between the downstream drift chamber and final TSC module with a measurement using events from single-track trigger runs.

Table I gives the ratios of weighted acceptances $A_{\mu\mu}^{\pi\pi}$ for each fitter, which multiplied by $(N_{\mu\mu}/PN_{\pi\pi})$ gives the branching ratio $B_{\pi\pi}^{\mu\mu}$. Additional systematic errors were estimated by studying the variation of the branching ratio as a function of cut values for the track and vertex χ^2 and the low mass limit of the signal region. This additional error of 0.45% and 0.30% for the FT and QT fitters, respectively, was added in quadrature to $A_{\mu\mu}^{\pi\pi}$. Uncertainties in the survey positions and counter efficiencies of the trigger scintillators, creating potential bias between $\mu^+\mu^-$ and $\pi^+\pi^-$ decay modes, led to further systematic errors in $A_{\mu\mu}^{\pi\pi}$ of 0.38% and 0.12%, respectively. The resulting branching ratios for the FT and QT fitters (Table I) differ by 0.006×10^{-6}, or 0.2%.

To determine a final branching ratio, the central $B_{\pi\pi}^{\mu\mu}$ value of the two fitters was chosen. An additional systematic error of one-half the fitter difference was added in quadrature to give $B_{\pi\pi}^{\mu\mu} = (3.474 \pm 0.057) \times 10^{-6}$. Multiplying this result by the measured value $B(K_L^0 \to \pi^+\pi^-) = (2.067 \pm 0.035) \times 10^{-3}$ [3] gives a final $\mu^+\mu^-$ branching fraction of $B(K_L^0 \to \mu^+\mu^-) = (7.18 \pm 0.17) \times 10^{-9}$. This result agrees with the average value from previous measurements [3], and reduces the experimental uncertainty on the branching fraction by a factor of 3.

Subtracting the unitarity bound for the ratio of partial widths $\Gamma(K_L^0 \to \gamma\gamma \to \mu^+\mu^-)/\Gamma(K_L^0 \to \pi^+\pi^-) = (3.421 \pm 0.067) \times 10^{-6}$ from our improved branching ratio (which takes proper account of correlations in different quantities [10]) implies a value for the dispersive contribution to the decay rate of $(0.11 \pm 0.18) \times 10^{-9}$, or $|\mathrm{Re}A_{\mathrm{exp}}|^2 < 0.37 \times 10^{-9}$ (90% C.L.). Using a recent estimate [7] of the magnitude of the long-distance dispersive amplitude $|\mathrm{Re}A_{\mathrm{LD}}| < 2.9 \times 10^{-5}$ (90% C.L.) to derive a lower bound on the Wolfenstein parameter ρ, we find that $\rho > -0.33$ (90% C.L.), which is consistent with existing constraints [5].

We acknowledge the support of the BNL staff, particularly H. Brown, R. Brown, R. Callister, F. Kobasiuk, W. Leonhardt, M. Howard, J. Negrin, and J. Scaduto. M. Hamela, D. Ouimette, S. Kettell, and R. Atmur played key roles in the design and fabrication of important parts of the experiment. C. Allen, G. Bowden, P. deCecco, P. Coffey, M. Diwan, K. M. Ecklund, M. Marcin, C. Nguyen, A. Schwartz, B. Ware, E. Wolin, and S. Worm made important contributions during the early phases of the experiment. We thank V. Abadjev, P. Gill, N. Mar, J. Meo, M. Roehrig, and M. Witkowski for valuable technical assistance. We also thank the SLAC Computing Division and the BNL CCD for assistance with data processing. This work was supported in part by the U.S. Department of Energy, the National Science Foundation, the Robert A. Welch Foundation, and Research Corporation.

[1] S. L. Glashow, J. Iliopoulos, and L. Maiani, Phys. Rev. D **2**, 1285 (1970).
[2] L. M. Sehgal, Phys. Rev. **183**, 1511 (1969).
[3] Particle Data Group, C. Caso *et al.*, Eur. Phys. J. C **3**, 1 (1998).
[4] C. Q. Geng and J. N. Ng, Phys. Rev. D **41**, 2351 (1990).
[5] A. J. Buras and R. Fleischer, hep-ph/9704376.
[6] L. Wolfenstein, Phys. Rev. Lett. **51**, 1945 (1983).
[7] G. D. D'Ambrosio, G. Isidori, and J. Portolés, Phys. Lett. B **423**, 385 (1998).
[8] D. G. Dumm and A. Pich, Phys. Rev. Lett. **80**, 4633 (1998).
[9] G. Valencia, Nucl. Phys. **B517**, 339 (1998).
[10] A. P. Heinson *et al.*, Phys. Rev. D **51**, 985 (1995).
[11] D. Ambrose *et al.*, Phys. Rev. Lett. **81**, 4309 (1998).
[12] D. Ambrose *et al.*, Phys. Rev. Lett. **81**, 5734 (1998).
[13] S. Graessle *et al.*, Nucl. Instrum. Methods Phys. Res., Sect. A **367**, 138 (1995).
[14] J. Belz *et al.*, Nucl. Instrum. Methods Phys. Res., Sect. A **428**, 239 (1999).
[15] After removing the blind prescale, the efficiencies $\varepsilon_{\mu\mu}^{\mathrm{TSC}}$, $\varepsilon_{\pi\pi}^{\mathrm{TSC}}$, and $\varepsilon_{\pi\pi}^{\mathrm{ABS}}$ were recalculated to reduce systematics, resulting in a 0.7% decrease in the branching ratio.
[16] D. A. Dicus and W. W. Repko, Phys. Rev. D **59**, 094018 (1999).
[17] H. Taureg *et al.*, Phys. Lett. **65B**, 92 (1976).